processes

MDPI

Article

Evaluation of Caprock Sealing Performance for CO_2 Saline Aquifer Storage: A Numerical Study

Xiaohan Shu [1,2,*], Lijun Zhang [1,2], Lei Zhang [3], Xiabin Wang [1,2], Xiaofeng Tian [1,2] and Lingdong Meng [4]

[1] State Key Laboratory of Offshore Oil and Gas Exploitation, Beijing 102200, China
[2] Development and Research Department of CNOOC Research Institute, Beijing 102200, China
[3] CNOOC (China) Limited Tianjin Branch, Tianjin 300450, China
[4] Bohai Rim Energy Research Institute, Northeast Petroleum University, Qinghuangdao 066004, China
* Correspondence: shuxh@cnooc.com.cn

Abstract: The integrity of caprock sealing is a crucial factor in guaranteeing the safety and long-term feasibility of CO_2 saline aquifer storage. In this study, we identified three principal mechanisms that give rise to topseal failure: (1) gradual CO_2 seepage through the upper cap, (2) capillary seal failure resulting from the pressure increment due to CO_2 injection, and (3) localized overpressure causing cap rupture. Through the integration of numerical simulation and geomechanics, this study offers a sealing assessment for the caprock. The thorough analysis of the sealing performance of the Guantao formation reveals that after 2000 years of CO_2 injection, the caprock would undergo intrusion by 35 m without any leakage risk. Moreover, investigations into CO_2–water–rock interactions suggest that precipitation reactions outweigh dissolution reactions, leading to a decreased permeability and an enhanced sealing performance. The most likely fracture mode identified is shear fracture with a critical caprock fracture pressure of 36.48 MPa. In addition to these discoveries, it is significant to consider ongoing research aimed at enhancing our ability to predict and manage potential risks associated with carbon capture and storage technologies.

Keywords: CO_2 saline aquifer storage; sealing performance; caprock; CO_2 transport; sealing site selection; mechanical integrity; main controlling factors; CO_2–water–rock interaction

check for updates

Citation: Shu, X.; Zhang, L.; Zhang, L.; Wang, X.; Tian, X.; Meng, L. Evaluation of Caprock Sealing Performance for CO_2 Saline Aquifer Storage: A Numerical Study. *Processes* **2024**, *12*, 1727. https://doi.org/10.3390/pr12081727

Academic Editor: Salman Soltani

Received: 18 July 2024
Revised: 8 August 2024
Accepted: 12 August 2024
Published: 16 August 2024

Copyright: © 2024 by the authors. Licensee MDPI, Basel, Switzerland. This article is an open access article distributed under the terms and conditions of the Creative Commons Attribution (CC BY) license (https://creativecommons.org/licenses/by/4.0/).

1. Introduction

The increasing threat posed by greenhouse gas emissions has made global warming a critical challenge of the 21st century. Despite our reliance on fossil fuels such as oil, natural gas, and coal, saline aquifer storage has emerged as an effective approach for reducing atmospheric CO_2 levels [1–3]. Efficient, safe, and economically feasible carbon dioxide sequestration is a highly valuable and complex research goal. In recent years, there has been growing interest in exploring alternative methods for reducing greenhouse gas emissions beyond traditional carbon capture and storage techniques. Researchers have been investigating innovative approaches such as direct air capture technology, bioenergy with carbon capture and storage (BECCS), and enhanced weathering to complement existing strategies [4–6]. Furthermore, international collaboration and investment in large-scale demonstration projects are crucial for advancing the deployment of carbon sequestration technologies [7,8]. In our urgent efforts to mitigate the impacts of climate change, it is crucial to prioritize sustainable solutions that can effectively reduce CO_2 emissions without compromising energy security or economic development [9,10].

The integrity and effectiveness of CO_2 sequestration are significantly influenced by geological discontinuity, CO_2–water–rock reactions, and extreme conditions of temperature, pressure, and stress within deep saline aquifers [11]. Current research primarily focuses on caprock properties such as thickness, permeability, porosity, and capillary pressure [12–15]. According to Fu et al., greater caprock thickness, broader horizontal distribution, and enhanced airtightness are associated with improved containment efficacy [16]. Jiang et al.

stress that the primary sealing mechanisms of the cap layer are capillary sealing and permeation sealing. Capillary sealing occurs at the CO_2–brine interface, preventing any upward flow of CO_2. Permeation sealing takes place when the breakthrough pressure is exceeded with the cap layer serving as a barrier to permeation. While both mechanisms exhibit limited leakage, they persist over an extended period [17].

Studies have also investigated the movement of CO_2 under various reservoir conditions. Li et al.'s research on sandstone reservoirs in Ordos demonstrates that both the permeability of the reservoir and the pressure–temperature conditions influence the migration of CO_2 [18]. Cui examined how reservoir permeability distribution and temperature impact the stable burial efficiency of CO_2 saline aquifers by establishing a comprehensive characterization index for burial efficiency, using numerical simulation and Pearson correlation coefficient statistics [19].

While these studies provide a theoretical basis, their practical application is still constrained. Diao et al. established a geological safety evaluation system and determined that the impermeability and mechanical stability of the caprock are of significant importance, indicating that a stable regional caprock is crucial for ensuring successful CO_2 geological storage [20]. However, there is still a lack of comprehensive studies that integrate both physical properties and CO_2–water–rock reactions.

This study thoroughly examines the intricate dynamics of the saline aquifer within the Guantao formation, which is located within an oilfield of the Bohai Sea. Through a detailed assessment of CO_2–water–rock interaction, this research aims to elucidate the interplay between these elements and their impact on subsurface geological formations. Using numerical simulation methods, it seeks to evaluate the sealing effectiveness of the Ming-Huazhen formation cap layer. Furthermore, by integrating geomechanics techniques with numerical simulations, this study aims to examine potential risks associated with hydraulic fracturing and CO_2 injection-induced leakage in the caprock. The analysis encompasses both dynamic and static perspectives, providing a robust foundation for optimizing the location and deepening our insights into more effective strategies for utilizing and strengthening the sealing layer in this geological setting.

2. Geological Setting

The Guantao Formation in the Bohai Sea region exhibits a stable geological structure characterized by significant sand body thickness (510–650 m) and high porosity and permeability. The overlying Minghuazhen Formation's mudstone cap layer, approximately 40 m thick, serves as a reliable seal. Faults are rarely observed within both the cap layer and storage unit. The formation pressure is calculated to be 23.92 MPa, with a temperature of 97 °C, which maintains the CO_2 in a supercritical state.

The basic physical properties of the reservoir are shown in Tables 1 and 2. The water quality indicators and rock mineral composition of formation water are shown in Tables 3 and 4. These reservoir parameters will be input into the model. The parameter values in the model come from the data of a single well, and the reservoir has heterogeneity. It is possible that the data of this well cannot fully represent the reservoir parameters, which will affect the accuracy of the model results. We recommend using data from multiple wells for a more practical scenario.

Table 1. Basic parameters of reservoir model.

Type	Value
Bottom hole pressure	32 MPa
Temperature	97 °C
Salinity	0.99 NaCl ($CaCl_2$ of Water type)
CO_2 injection rate	6.5 kg/s, 4.0 kg/s, 1.5 kg/s (562 t/d, 350 t/d, 130 t/d)

Table 2. Geological parameters of cap rock and reservoir.

Type	Target Stratum	
	Mudstone Caprock	**Sandstone Formation**
Permeability (m^2)	1.00×10^{-18}	5.80×10^{-13}
Porosity (%)	5	17
CO_2 injection rate (wt.%)	0.99	0.99
Residual water saturation	0.3	0.15
Residual gas saturation	0.05	0.1
Maximum water saturation	0.99	0.99
Maximum gas saturation	0.99	0.99
Capillary pressure (MPa)	0.0621	0.0196

Table 3. Ionic composition and concentration of saline water.

Concentration (mol/kg)						
K^+	Na^+	Mg^{2+}	Ca^{2+}	Cl^-	$SO_4{}^{2-}$	$HCO_3{}^-$
1.15×10^{-3}	0.17	4.167×10^{-4}	5.65×10^{-3}	0.1745	1.146×10^{-4}	5.403×10^{-3}
Mineralizaion (mg/L)			Water Type		pH	
10,769			$CaCl_2$		7.48	

Table 4. Rock mineral composition.

Type	Target Stratum	
	Formation	**Caprock**
Calcite	3	7
Quartz	43	40
Kaolinite	0	4
Illite	0	7
Low-albite	17	10
Smectite-Na	15	24
K-feldspar	17	3
Chlorite	5	5

3. Methodology

Two key factors primarily influence the caprock sealing performance: capillary sealing and hydraulic sealing. The capillary pressure threshold is affected by pore throat size, wettability, and CO_2–water surface tension. Numerical simulation can be used to study capillary breakthrough, taking into account pressure, temperature, chemical changes, and the mechanical response of the rock. Hydraulic sealing can be evaluated through the construction of a stress field model to identify failure conditions and guide field applications.

3.1. Numerical Simulation of Thermo-Hydro-Mechanical–Chemical (THMC)

Physical experiments related to the geomechanics response and CO_2 migration and transformation laws are typically limited to small spatial scales (<1 m) and short time spans (<30 day). This limitation poses a challenge in elucidating the CO_2 sequestration mechanisms at the stratigraphic scale. However, numerical experiments can comprehensively consider the physical and chemical interactions of CO_2–water–rock over extensive spatiotemporal ranges, offering a more comprehensive understanding.

The phase state of CO_2 is determined by temperature and pressure, while the physical and chemical interactions between CO_2, water, and rock are influenced by temperature. The behavior of multiphase flow involving water and CO_2, as well as the coupling of flow pressure/velocity distribution with chemical fields, stress fields, and temperature fields, have a significant impact on CO_2 storage efficiency and long-term safety. The chemical field primarily considers the physical and chemical reactions among CO_2, water, and rock.

While salt precipitation may reduce pore permeability, rock dissolution by H_2CO_3 may increase pore permeability along with changes in the mechanical properties of the rock. Under the combined effects of fluid pressure and original geostress, geological formations may deform and fail, leading to potential CO_2 leakage through activated joints, fractures, or faults which may compromise the integrity of CO_2 storage.

A fully coupled mathematical model has been developed based on the principles of THMC to simulate rock deformation, CO_2 migration, and temperature distribution during CO_2 injection. This model considers thermal conduction, flow, and deformation dynamics while incorporating the CO_2–water–rock interactions through a solute transport equation that includes chemical reactions for salt precipitation and dissolution.

3.1.1. Thermal Conduction

The phase behavior of CO_2 is influenced by temperature and pressure, while the physical and chemical interactions between CO_2, water, and rock are dependent on temperature. As a result, an overall energy conservation equation that accounts for thermal convection and conduction is formulated.

$$\frac{d}{dt}\int\limits_{V_n} M^\kappa \, dV_n = \int\limits_{\Gamma_n} E^\kappa \cdot n \, d\Gamma_n \, + \int\limits_{V_n} q^\kappa \, dV_n \tag{1}$$

where M^κ represents the total energy of solids and fluids

$$M^{NK+1} = (1-\phi)\rho_R C_R T + \phi \sum_\beta S_\beta \rho_\beta u_\beta \tag{2}$$

where E^κ represents the add-up of the heat conduction term and the heat convection term, which can be expressed as

$$E^{NK+1} = -\lambda \nabla \mathrm{T} + \sum_\beta h_\beta F_\beta \tag{3}$$

3.1.2. Flow Model

In accordance with the principles of CO_2 and brine migration and transformation, while taking into account convection and diffusion effects, the continuity equations for each component fluid can be formulated.

$$\frac{d}{dt}\int\limits_{V_n} P^\kappa \, dV_n = \int\limits_{\Gamma_n} F^\kappa \cdot n \, d\Gamma_n \, + \int\limits_{V_n} q^\kappa \, dV_n \tag{4}$$

where P^κ is the cumulative term of volumetric mass.

$$P^\kappa = \phi \sum_\beta S_\beta \rho_\beta X_\beta^\kappa \tag{5}$$

F^κ represents the convection and diffusion terms

$$F^\kappa|_{adv} = \sum_\beta X_\beta^\kappa \, F_\beta \tag{6}$$

$$F^\kappa|_{dis} = -\sum_\beta \rho_\beta \overline{D_\beta^\kappa} \nabla X_\beta^\kappa \tag{7}$$

3.1.3. Deformation Model

The mechanical response of rock deformation and discontinuous geological structures can be effectively described by the following stress expression.

$$\sigma_{ij} = \sigma'_{ij} + mp\delta_{ij} \tag{8}$$

Equilibrium equation of rock mass continuous medium

$$\sigma'_{ij,j} + f_i = 0 \tag{9}$$

Deformation equation

$$\varepsilon_{ij} = \frac{1}{2}(u_{i,j} + u_{j.i}) \tag{10}$$

Elastic–plastic constitutive equation

$$d\sigma'_{ij} = D^{ep}_{ijkl} d\varepsilon_{kl} \tag{11}$$

3.1.4. CO_2–Water–Rock Reaction

A solute transport equation incorporating chemical reactions to account for salt precipitation and dissolution effects between CO_2–water–rock can be formulated based on Equation (1).

A multi-component multiphase CO_2 migration THMC numerical model can thus be developed utilizing the finite element method and finite volume method. The specific calculation process is shown in Figure 1.

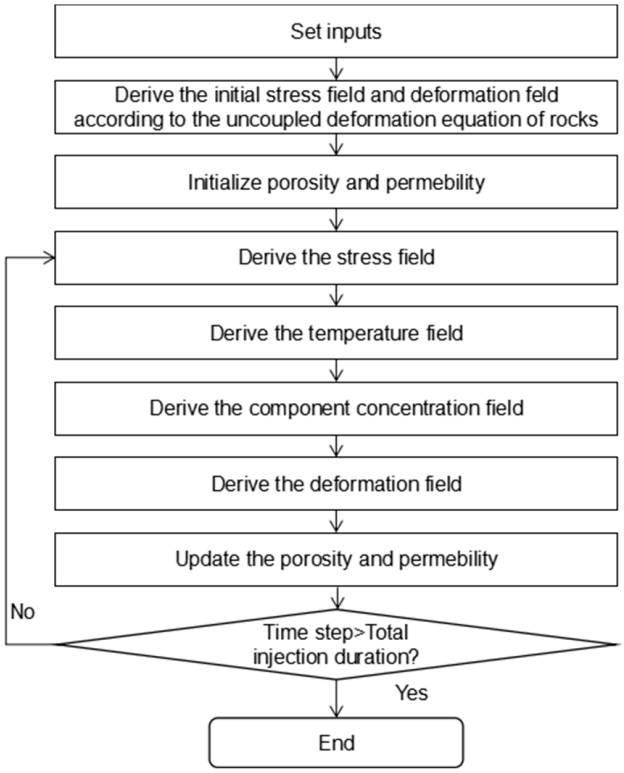


Figure 1. Flowchart of THMC model implementation.

3.2. Hydraulic Sealing Mechanics

The mechanical stability was evaluated using a stress field model to determine the activation pressure and fracture mechanics of the caprock with shear fracture identified as the primary failure mode.

3.2.1. Construction of Stress Field

Based on the stress analysis at the discontinuity level of the Mohr circle and its correlation with the rupture envelope, the additional fluid pressure can be formulated as

$$\Delta P = \sigma_n - (\tau - C)/\mu \tag{12}$$

The activation pressure can be expressed as

$$P_R = \Delta P + P_p \quad (13)$$

The activation pressure coefficient can be described as the ratio of activation pressure to static water pressure

$$P_{RC} = P_R / (\rho_w g h) \quad (14)$$

According to the leakage test from three wells, the relationship between three-dimensional stress and depth is obtained as follows: vertical principal stress S_v = 0.0203 h, maximum horizontal principal stress SH_{max} = 0.0208 h − 0.93, and minimum horizontal principal stress Sh_{min} = 0.0176 h − 2.34

3.2.2. Rupture Mechanics

Due to the lack of tensile strength data in the study area, that of the same layer in the nearby block is referenced (Table 5), which is 1.0 MPa. Applying the top depth of the cover, $\sigma_1 - \sigma_3$ = 14.09 MPa, which meets the condition of $(\sigma_1 - \sigma_3) > 6T$ stress according to the rock rupture criterion. Therefore, the cap rupture in the study area is shear rupture.

Table 5. Failure mechanics of cover layer (Mildren et al., 2005) [21].

Fracture Mode	Rock Fracture Criterion	Stress Condition
Tensional rupture (hydraulic rupture)	$P = \sigma_3 + T$	$(\sigma_1 - \sigma_3) < 4T$
Mixed rupture of tension and shear	$P = \sigma_n + (4T^2 - \tau^2)/4T$	$4T < (\sigma_1 - \sigma_3) < 6T$
Shear fracture	$P = \sigma_n + (C - \tau)/\mu$	$(\sigma_1 - \sigma_3) > 6T$

4. Result and Discussion

4.1. CO_2 Migration and Caprock Intrusion

Base on the typical reservoir profile in the Field A area, a two-dimensional model was established with a cap layer thickness of 40 m (Figure 2). The injection point was designed to be 60 m below the top surface of the reservoir, as shown in Figure 3. Subsequently, it was initialized based on the actual hydrogeological parameters, mineral components of the formation, and chemical components of the aqueous solution. Injection boundary conditions, outflow boundary conditions, and initial conditions were defined for conducting numerical simulation of CO_2–water–rock chemical reaction heat–chemistry–flow–solidity over an injection period of 30 years.

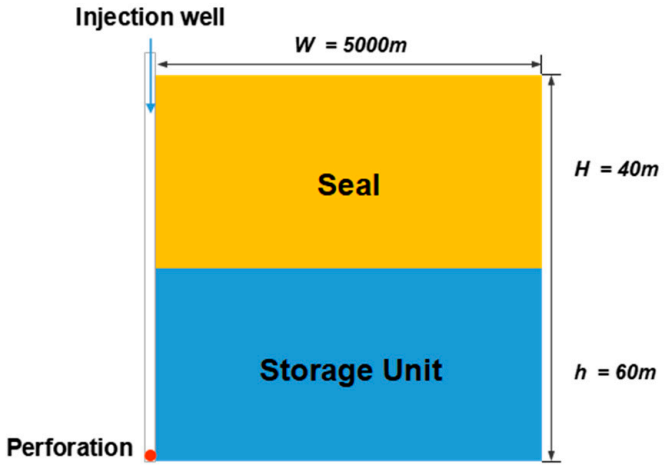


Figure 2. Schematic simplified model of Field A Guantao Formation.

During the initial 30 years, CO_2 injection continued, resulting in a lateral migration distance of approximately 600 m at the bottom and an increasing migration distance at

the top over time. By the 300-year mark, the distribution pattern of CO_2 had stabilized with no significant changes in migration distance observed from then until the 2000-year mark. Throughout the injection period, CO_2 consistently infiltrated the caprock, reaching approximately 5 m after 30 years and nearly reaching the top of the caprock by the 2000-year mark. By that year, the maximum intrusion distance of dissolved CO_2 into the caprock had reached about 35 m at an extremely low intrusion rate.

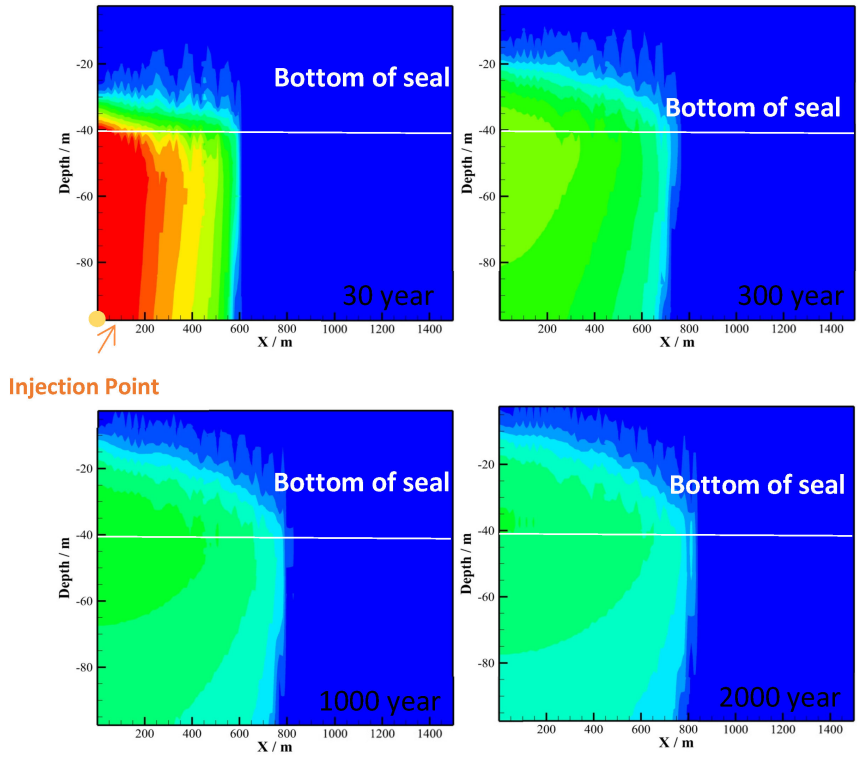


Figure 3. CO_2 plume intrusion into the caprock in 2000.

During the initial 30 years, the lateral spread of CO_2 at the depth of injection was approximately 600 m, while the transport distance near the caprock gradually increased over time. After 300 years, the distribution of CO_2 stabilized, and there were no significant changes in migration distances from then until the 2000-year mark. Throughout the injection process, CO_2 seeped into the caprock, reaching around 5 m within 30 years. By 1000 years, the dissolved CO_2 had migrated approximately 35 m, reaching almost to the top of the caprock. This slow seepage continued until the 2000-year mark.

4.2. CO_2–Water–Rock Interaction

The CO_2–water–rock interaction within the caprock was simulated numerically. The pH of the brackish water showed a significant decrease immediately after the start of the injection, followed by an increase after 1000 years, and then showed minimal variation. The concentration of HCO_3^- in solution gradually increased, indicating an increasing dissolution of CO_2. Calcite, potassium feldspar, and chlorite all underwent dissolution reactions with calcite and chlorite demonstrating increased dissolution over time. Magnesite underwent a precipitation reaction, leading to greater precipitation with prolonged duration. Owing to the prevalence of precipitation reactions over time, the porosity and permeability of the caprock were notably diminished (Figure 4). Based on these findings, we infer that the CO_2–water–rock interaction in the caprock has a negligible impact on its capillary sealing capacity, resulting in an extremely low risk of caprock leakage.

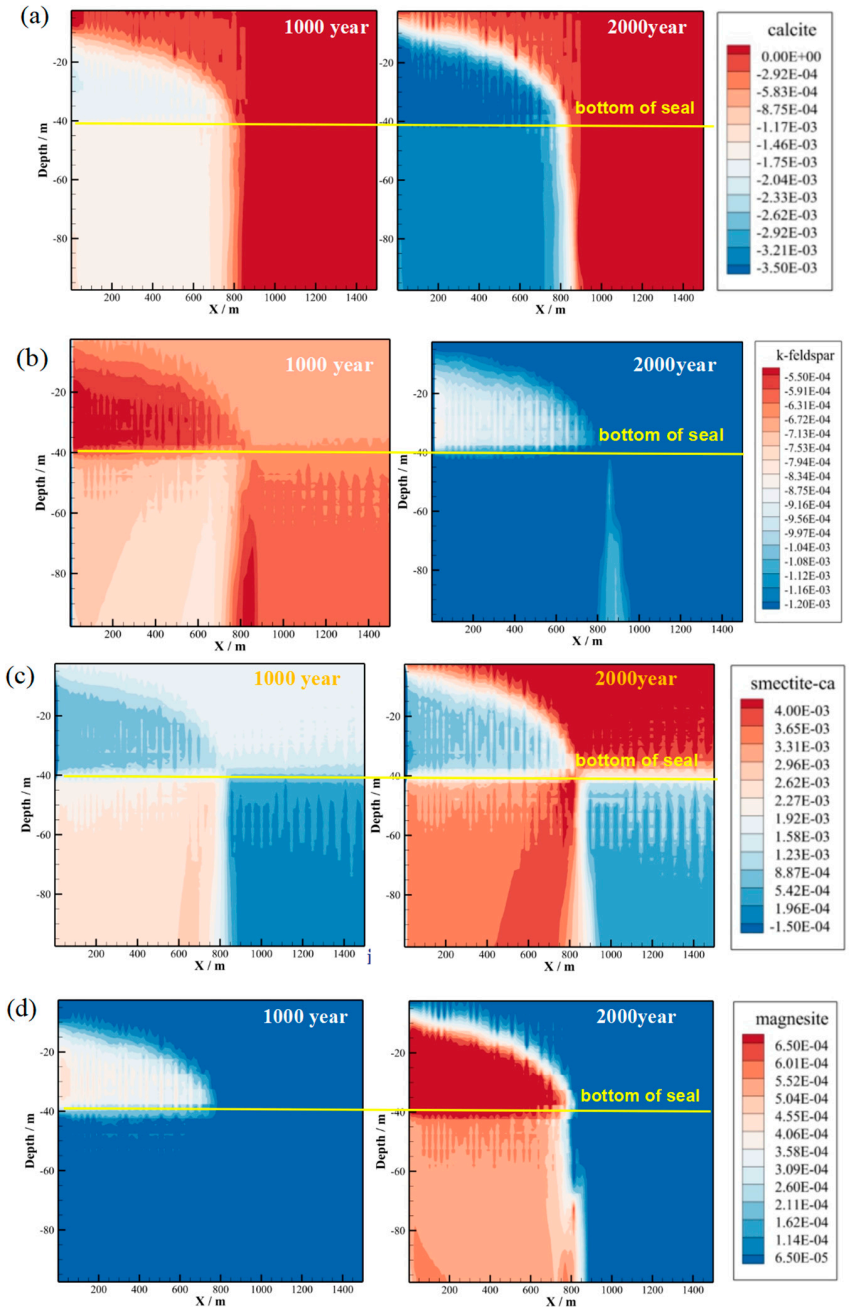


Figure 4. Degree of CO_2–water–rock interaction. (**a**) Calcite Dissolution; (**b**) K -Feldspar Dissolution; (**c**) Ca -Montmorillonite Precipitation; (**d**) Magnesite Precipitation.

4.3. Hydraulic Fracturing Risk

Through three-dimensional geological modeling, we have utilized caprock data and stress field information specific to our research site to develop a comprehensive model. This model depicts hydraulic fracturing pressures within T0 reflector layers. Due to minimal depth variations across the various layers of the cover, wide-ranging color codes fail to distinctly highlight weaknesses in their hydraulic seal capabilities. To reveal these vulnerabilities, we employ a single-layer assessment approach. By simulating and computing caprock's top-to-bottom hydraulic seal capacities for each stratum using stress fields, we derive fracture pressure values within respective ranges—thus enabling a quantitative evaluation of caprock's overall sealing performance in this region (Figure 5).

The top depth of the cover layer on the surface of the Guantao formation is 2270 m. Based on the hydraulic fracturing pressure plan and stress Mohr circle at this depth, the

fracturing pressure is calculated to be 36.48 MPa with a fracturing pressure coefficient of 1.61. The bottom depth of the top cover layer on the Guantao Formation is 2345 m. According to the hydraulic fracturing pressure plan and stress Mohr circle at this depth, the calculated fracturing pressure for the top cover layer on the Guantao formation is 37.61 MPa with a fracturing pressure coefficient of 1.60 (Figure 6).

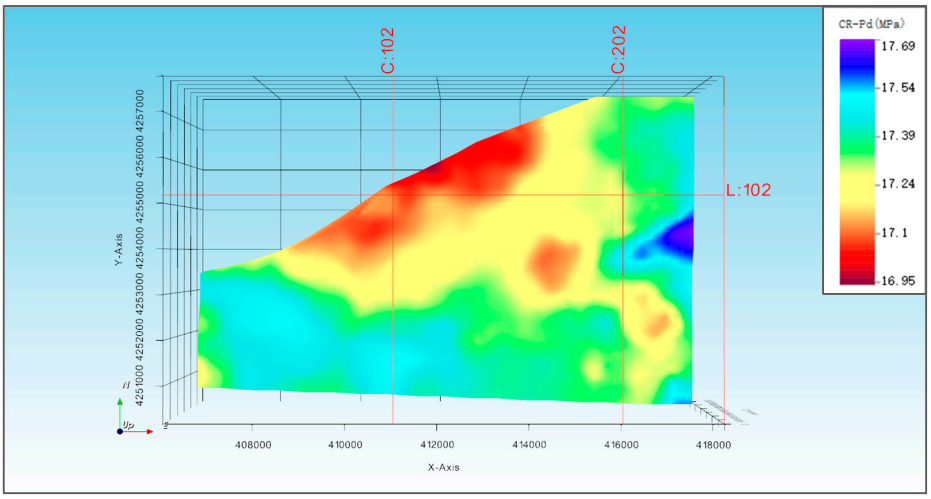


Figure 5. Distribution of hydraulic fracturing pressure of the Guantao Formation.

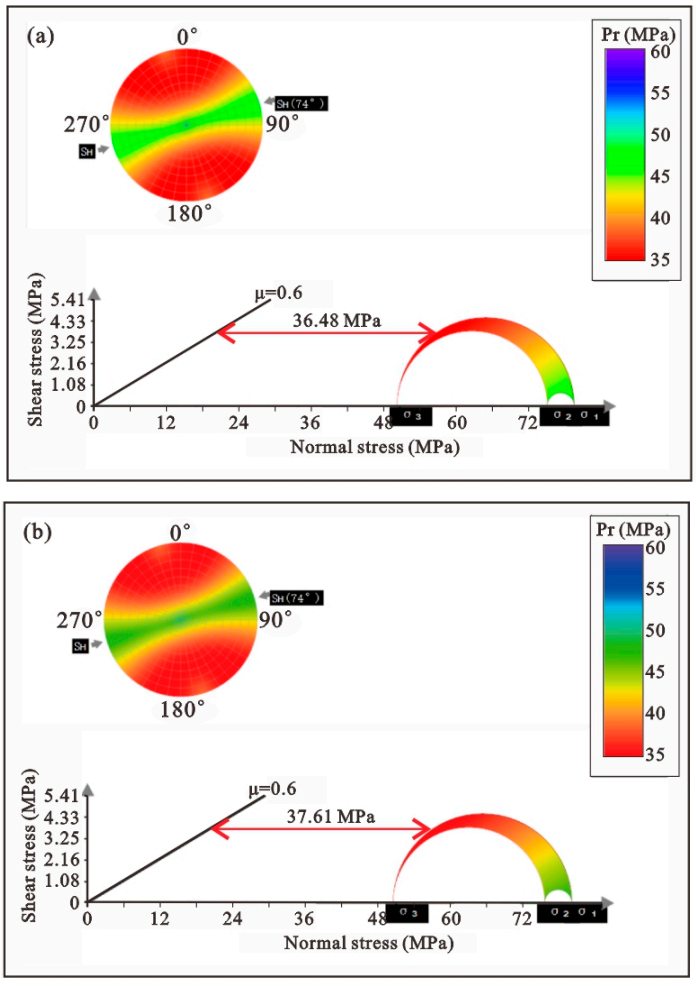


Figure 6. Stress field of the cover layer on the upper surface of the Guantao Formation. (**a**) The top depth; (**b**) The bottom depth.

In conclusion, with increasing burial depth, the hydraulic fracturing pressure of the caprock gradually rises, resulting in the highest risk of fracturing at the top depth of the caprock. The minimum fracturing pressure of the caprock in this area is 36.48 MPa.

5. Conclusions

The integrated numerical simulation of THMC processes comprehensively takes into account temperature distribution, rock deformation, crack/fault activation, and CO_2–water–rock physical and chemical reactions during and after CO_2 saline aquifer storage injection. This approach facilitates the assessment of CO_2 phase change, rock mechanics analysis, fault and cap sealing evaluation, as well as prediction of permeability changes in the cap and reservoir. In addition, it offers guidance for calculating the CO_2 storage capacity and optimizing the design parameters for saline aquifer storage engineering.

The thick overlying mudstone cap layer of the Guantao Formation in the Field A area exhibits excellent sealing properties. The simulation results indicate that following 2000 years of CO_2 injection, the caprock would experience an intrusion of approximately 35 m without any leakage. This demonstrates a stable CO_2 distribution pattern and minimal migration distance beyond 300 years. The interaction between CO_2, water, and rock primarily involves the dissolution of calcite, potassium feldspar, and chlorite with precipitated magnesite contributing to reduced caprock permeability and enhanced sealing capacity. The hydraulic fracturing pressure of the caprock increases with depth. At the top of the caprock, a minimum fracturing pressure of 36.48 MPa was identified. Shear was identified as the primary fracture mode, indicating a low risk of hydraulic failure under current conditions.

Author Contributions: X.S.: Conceptualization, funding acquisition, project administration, resources, software and writing—original draft, and writing—review and editing. L.Z. (Lijun Zhang): Data curation, formal analysis, methodology, writing—original draft, and writing—review and editing. L.Z. (Lei Zhang): Project administration, resources. X.W.: Investigation, methodology, software, and visualization. X.T.: Conceptualization, funding acquisition, methodology. L.M.: Investigation, methodology, project administration. All authors have read and agreed to the published version of the manuscript.

Funding: This work was support by the National Natural Science Foundation of China (U23B2090), National Key R&D Program of China (2023YFB4104200), and the CNOOC's "14th Five-Year Plan" major science and technology project (KJGG-2022-12-CCUS-0203).

Data Availability Statement: The original contributions presented in the study are included in the article, further inquiries can be directed to the corresponding author.

Conflicts of Interest: Author Zhanglei is employed by CNOOC (China) Limited Tianjin Branch. The remaining authors declare that the research was conducted in the absence of any commercial or financial relationships that could be construed as a potential conflict of interest.

References

1. Yu, G.; Hao, T.; Zhu, J. Discussion on action strategies of China's carbon peak and carbon neutrality. *Bull. Chin. Acad. Sci.* **2022**, *37*, 423–434. (In Chinese)
2. Zhang, X.; Li, Q.; Wang, Z. Evaluation of suitability and planning strategy of carbon sequestration in national land space at city and county level. *J. Small Town Constr.* **2022**, *40*, 16–23.
3. Lv, S.-H. Current status and comparison of the development of geologic CO_2 sequestration technology. *J. Yunnan Chem. Ind.* **2022**, *9*, 69–71.
4. Keller, D.P.; Lenton, A.; Scott, V.; Vaughan, N.E.; Bauer, N.; Ji, D.; Jones, C.D.; Kravitz, B.; Muri, H.; Zickfeld, K. The carbon dioxide removal model intercomparison project (CDRMIP): Rationale and experimental protocol for CMIP6. *Geosci. Model Dev.* **2018**, *11*, 1133–1160. [CrossRef]
5. Hester, T. Legal pathways to negative emissions technologies and direct air capture of greenhouse gases. *Envtl. L. Rep. News Anal.* **2018**, *48*, 10413.
6. Schäfer, S.; Lawrence, M.; Stelzer, H.; Born, W.; Low, S.; Aaheim, A.; Adriázola, P.; Betz, G.; Boucher, O.; Carius, A.; et al. *The European Transdisciplinary Assessment of Climate Engineering (EuTRACE). Removing Greenhouse Gases from the Atmosphere and Reflecting Sunlight away from Earth*; EuTRACE: Berlin, Germany, 2015.

7. De Blasio, N.; Krishnamoorthy, S.; Kapadia, Z.; Mayer, A.; Schiele, J.; Sweeney-Taylor, A. *Deploying Energy Innovation at Scale for a Low-Carbon Economy: The Private Sector Role-ENGIE; Environment and Natural Resources Program Papers*; Belfer Center for Science and International Affairs, Harvard Kennedy School: Cambridge, MA, USA, 2020.
8. Miocic, J.M.; Heinemann, N.; Alcalde, J.; Edlmann, K.; Schultz, R.A. Enabling secure subsurface storage in future energy systems: An introduction. *Geol. Soc. Lond. Spec. Publ.* **2023**, *528*, 1–4. [CrossRef]
9. Batra, G. Renewable energy economics: Achieving harmony between environmental protection and economic goals. *Soc. Sci. Chron.* **2023**, *2*, 1–32. [CrossRef]
10. Zohuri, B. Navigating the global energy landscape balancing growth, demand, and sustainability. *J. Mat. Sci. Apl. Eng.* **2023**, *2*, 1–7.
11. Skurtveit, E.; Miri, R.; Hellevang, H. Fluid-Rock Interactions in Clay-Rich Seals: Impact on Transport and Mechanical Properties. In *Geological Carbon Storage: Subsurface Seals and Caprock Integrity*; Wiley: Hoboken, NJ, USA, 2018; pp. 167–185.
12. Song, J.; Dong, X. Comprehensive review of caprock-sealing mechanisms for geologic carbon sequestration. *J. Environ. Sci. Technol.* **2012**, *10*, 301610. [CrossRef] [PubMed]
13. Suekane, T.; Izumi, T.; Okada, K. Capillary trapping of supercritical CO_2 in porous media at the pore scale. *J. Multiph. Flow* **2011**, *1*, 110261.
14. Li, G. Numerical investigation of CO_2, storage in hydrocarbon field using a geomechanical-fluid coupling model. *J. Pet.* **2016**, *2*, 252–257. [CrossRef]
15. Cinar, Y. Carbon dioxide sequestration in saline formations: Part 2-Review of multiphase flow modeling. *J. Pet. Sci. Eng.* **2014**, *124*, 381–389. [CrossRef]
16. Fu, X.; Wu, T.; Lu, Y. Current status and future development trend of oil and gas reservoir cap closure research. *J. Oil Gas Geol.* **2018**, *39*, 454–471.
17. Jiang, Y. Discussion on the relationship between the thickness of oil and gas reservoir cover and the height of capped hydrocarbon column. *J. Nat. Gas Ind.* **1998**, *2*, 30–33.
18. Li, X.; Chang, C.; Guo, J. Experimental study on CO_2, capillary residual sequestration capacity of Ordovician reef tuffs in the Tarim Basin. *J. Geol. Front.* **2011**, *18*, 190–194.
19. Cui, C.; Zhang, T.; Zhang, C. Stable burial efficiency of CO_2 in saline formation and optimization of reservoir parameters. *J. Daqing Pet. Geol. Dev.* **2023**, *42*, 141–147.
20. Diao, Y.; Zhang, S.; Guo, J. Research on evaluation method of geosafety of geological storage in deep saline aquifer CO_2. J. *China Geol.* **2011**, *38*, 786–792.
21. Mildren, S.D.; Hillis, R.R.; Dewhurst, D.N.; Lyon, P.J.; Meyer, J.J.; Boult, P.J. *FAST: A New Technique for Geomechanical Assessment of the Risk of Reactivation-Related Breach of Fault Seals*; The American Association of Petroleum Geologists: Tulsa, OK, USA, 2005.

Disclaimer/Publisher's Note: The statements, opinions and data contained in all publications are solely those of the individual author(s) and contributor(s) and not of MDPI and/or the editor(s). MDPI and/or the editor(s) disclaim responsibility for any injury to people or property resulting from any ideas, methods, instructions or products referred to in the content.